In silico computational investigation of compounds from *Scutellaria baicalensis* as potential inhibitors of A42R, scaffold protein D13, and mpox virus DNA polymerase through semi-empirical QM, MEP, PCA, FEL, and RIN approaches

Wirdatun Nafisah[1,*], Gusnia Meilin Gholam [2], Riyan Alifbi Putera Irsal[3], Fatima Shahid[4,5], Erwince Fallo[2], Josephine Elizabeth Siregar[6], Syahputra Wibowo[6], Wakhid Wakhid[7]

[1] Biology Department, Faculty of Mathematics and Natural Science, Universitas Negeri Surabaya, Indonesia

[2] Department of Biochemistry, Faculty of Mathematics and Natural Sciences, IPB University, Bogor, Indonesia

[3] Department of Applied Chemistry, Faculty of Engineering, Kyushu University, Japan

[4] Department of Applied Physics, Faculty of Science and Technology, FST, University Kebangsaan Malaysia (UKM), Malaysia;

[5] Department of Industrial Biotechnology, Atta Ur Rahman School of Applied Biosciences, National University of Sciences & Technology, Islamabad, Pakistan

[6] Eijkman Research Center for Molecular Biology, National Research and Innovation Agency, Bogor, West Java, 16911, Indonesia

[7] Research Center for Applied Zoology, National Research and Innovation Agency, Bogor, West Java, 16911, Indonesia

[*]Corresponding author:

Wirdatun Nafisah

wirdatunnafisah@unesa.ac.id

Biology Department, Faculty of Mathematics and Natural Science, Universitas Negeri Surabaya, Indonesia

Abstract:

Introduction: Mpox remains an international public-health concern, while current antivirals are constrained by access, resistance, adverse effects, and limited clinical evidence. Natural flavonoids from Scutellaria baicalensis may provide complementary chemical scaffolds for targeting essential monkeypox virus (MPXV) proteins. To evaluate *S. baicalensis* constituents as inhibitors of the A42R profilin-like

protein, scaffold protein D13, and MPXV DNA polymerase using an integrated structure-based computational workflow.

Material and Methods: Receptors were prepared, validated by Ramachandran analysis, and assessed with COACH-D. Nineteen semi-empirically optimized phytochemicals were screened by docking, interaction mapping, MEP analysis, and ProTox-3. Selected complexes underwent 10 ns molecular dynamics simulations followed by RMSD, PCA, DCCM, FEL, NMA, RIN, and Protein Contact Atlas analyses.

Result: All receptors had more than 90% favored residues. Scutellarein-7-O-diglucuronide showed the highest binding energies for A42R (8.265 kcal/mol) and D13 (11.416 kcal/mol); Norwogonoside and Oroxyloside led for DNA polymerase (10.022 kcal/mol). Scutellarein-7-O-diglucuronide and Norwogonoside were toxicity class 5 and inactive across the evaluated endpoints. Dynamic analyses supported stable interaction networks with target-dependent conformational adaptation.

Conclusion: Scutellarein-7-O-diglucuronide and Norwogonoside are prioritized as computationally supported, natural-product-based candidates for experimental anti-MPXV evaluation. The novelty and broader implications of this study lie in its multi-target strategy, which addresses molecular targets involved in different stages of the mpox virus life cycle. Furthermore, advanced in silico computational approaches were integrated to identify and evaluate the proposed inhibitory compounds.

Keywords: Flavonoid; Molecular dynamics simulation; Mpox therapeutics; Structure-based drug discovery; Toxicity prediction

1. Introduction

Mpox is a zoonotic disease caused by monkeypox virus (MPXV), a double-stranded DNA orthopoxvirus. Its expansion beyond historically endemic regions during and after the 2022 outbreak established sustained human-to-human transmission and imposed substantial clinical and socioeconomic burdens [1]. Typical manifestations include fever, lymphadenopathy, myalgia, and progressive skin lesions, with severe disease occurring disproportionately in immunocompromised individuals, children, and other vulnerable groups. Transmission remains ongoing; in March 2026, 48 countries reported 1,235 confirmed cases and five deaths, with clade Ib detected in newly affected settings and community transmission documented outside Africa [2,3].

Vaccinia-derived vaccines, including MVA-BN and ACAM2000, provide cross-protection, but access and suitability vary across populations and regions [4]. Therapeutic options are likewise limited by unequal availability, incomplete evidence of long-term effectiveness, potential resistance, and treatment-related adverse effects, including liver-enzyme elevation associated with brincidofovir [5]. These constraints support the search for compounds that act on essential viral proteins and may contribute to multi-target therapeutic strategies.

Recent computational studies have shown that MPXV proteins are tractable targets for antiviral discovery. Virtual screening against the A42R profilin-like protein, followed by molecular dynamics and MM/PBSA analysis, identified compounds with favorable predicted binding and stability [6]. A later repurposing study targeting the VP39 2′-O-methyltransferase similarly identified approved antivirals with promising docking, simulation, and MM-GBSA profiles [7]. However, these investigations relied primarily on single-target designs. The comparative behavior of structurally diverse natural products across MPXV proteins involved in distinct biological processes therefore remains insufficiently characterized.

A42R, the D13 scaffold protein, and DNA polymerase were selected because they represent complementary functions in host-associated viral activity, virion morphogenesis, and genome replication, respectively [8]. Their simultaneous evaluation provides a mechanistic basis for identifying compounds with target-specific or broader interaction profiles. *Scutellaria baicalensis* (*S. baicalensis*) is rich in flavonoids with reported antiviral, anti-inflammatory, antioxidant, and immunomodulatory activities. Its glycosides and aglycones, including baicalein, baicalin, wogonin, and scutellarein derivatives, have been investigated against several clinically important viruses and therefore constitute a relevant natural-product library for MPXV screening [9].

Accordingly, this study evaluated 19 reported S. baicalensis constituents against A42R, D13, and MPXV DNA polymerase using an integrated workflow encompassing

receptor validation, docking, toxicity prediction, molecular dynamics, and complementary post-simulation analyses [10]. The aim was to prioritize candidates with favorable target engagement, preliminary safety, and dynamic behavior for subsequent experimental validation.

2. Materials and methods

2.1 Receptor preparation

Three experimentally resolved receptors were obtained from the RCSB Protein Data Bank. A42R from MPXV Zaire-96-I-16 (PDB 4QWO; X-ray resolution 1.52 Å) contains two 157-residue chains [11]. Chain A and the native ligand PE8 were retained; chain B and water molecules were removed, hydrogen atoms were added, and pH was set to 9.0. Vaccinia virus D13 (PDB 6BED; 2.75 Å) comprises three 553-residue chains and was crystallized with rifampicin [12]. Chain A and rifampicin were retained, water was removed, hydrogens were added, and pH was set to 4.8. The MPXV DNA polymerase holoenzyme was derived from a 2.8 Å cryo-EM structure, with TTP retained as the reference ligand [13]. Each receptor was prepared in YASARA Structure, minimized with the AMBER14 force field, saved in PDB format, and evaluated using Ramplot to confirm backbone stereochemistry after preparation.

2.2 Ligand data and preparation

Nineteen *S. baicalensis* constituents were selected from the phytochemical compilation by Chanchal et al. [14]. Three-dimensional SDF structures were retrieved from PubChem, protonated and adjusted for pH in YASARA, optimized through the MOPAC semi-empirical quantum-mechanics procedure, and energy-minimized. The resulting structures were saved individually in PDB format and combined as a single ligands.sdf file for screening.

2.3 COACH-D binding-site analysis

Prepared receptor structures were submitted separately to COACH-D 2.0 in private mode. The server integrates TM-SITE, S-SITE, COFACTOR, FINDSITE, and ConCavity for monomeric targets and Q-SITE for multimeric structures. Predicted pockets, constituent residues, C-scores, and TM-scores were recorded and used to interpret docking poses.

2.4 Molecular docking

Docking was conducted in YASARA Structure with the VINA algorithm and AMBER14 parameters. Receptors were treated as rigid, and cubic grids surrounding all atoms were used because the study included binding-site prediction: 48.93 × 48.93 × 48.93 Å for A42R, 103 × 103 × 103 Å for D13, and 113.83 × 113.83 × 113.83 Å for DNA polymerase. The prepared ligands were screened using customized

dock_runscreening settings. YASARA binding energies were reported in kcal/mol, with larger positive values indicating more favorable predicted binding. The five highest-ranked compounds for each receptor were retained. Native ligands served as structural references, and two-dimensional interaction maps were generated in BIOVIA Discovery Studio.

2.5 MEP and toxicity analysis

The top-ranked ligands were analyzed in Avogadro using the MMFF94 force field, four optimization steps per update, and the steepest-descent algorithm. MEP surfaces were colored by electrostatic potential. Canonical SMILES from PubChem were then submitted to ProTox-3 to predict LD50, toxicity class, hepatotoxicity, neurotoxicity, cardiotoxicity, immunotoxicity, mutagenicity, and cytotoxicity.

2.6 Molecular dynamics simulation

Selected protein-ligand complexes were simulated for 10 ns with CABS-flex. Generated models were processed by normal-mode-based geometric simulation using large-scale motions and 1,000 simulation frames. Trajectories were analyzed in RStudio through RMSD distributions, PCA, DCCM, and FEL projections to characterize dominant conformations, collective motion, residue correlation, and low-energy states.

2.7 NMA, RIN, and Protein Contact Atlas analysis

The leading complex for each target was submitted to iMODS for coarse-grained Cα NMA with 20 deformation modes. RINmaker was used to construct residue interaction networks from PDB complexes without hydrogens or water. Hydrogen-bond and π-cation frequencies, distances, and energies were summarized. Protein Contact Atlas was used to visualize secondary-structure connectivity by chord plots and residue-network properties by scatter-plot matrices.

3. Results

3.1 Structural validation of A42R, D13, and MPXV DNA polymerase

Ramachandran analysis showed favorable post-preparation stereochemistry for all receptors (Figure 1). A42R contained 122 favored residues (92.424%), nine allowed residues (6.818%), and one disallowed residue (0.758%).

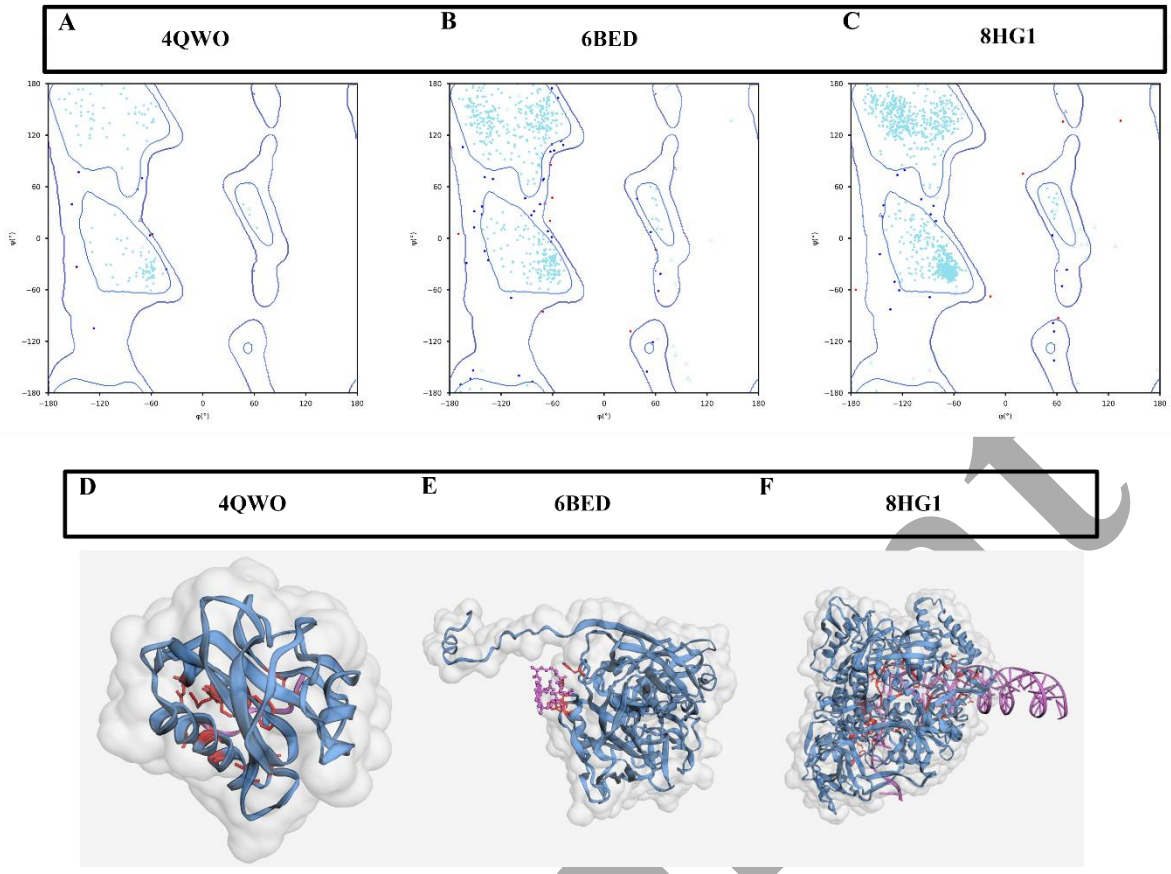

Figure 1. Post-preparation. Ramachandran plots for (A) A42R profilin-like protein, (B) scaffold protein D13, and (C) MPXV DNA polymerase after receptor preparation. COACH-D-predicted binding pockets for (D) A42R, (E) scaffold protein D13, and (F) MPXV DNA polymerase.

D13 contained 493 favored (91.296%), 40 allowed (7.407%), and seven disallowed residues (1.296%). DNA polymerase showed the highest favored proportion: 975 residues (97.305%), with 21 allowed (2.096%) and six disallowed residues (0.599%). Thus, each structure exceeded 90% favored residues and was retained for subsequent analysis (Figure 1A-1C).

3.2 Binding-site prediction

COACH-D predicted an A42R pocket with a C-score of 0.79 comprising W5, K7, I8, D11, L33, H125, R128, T132, and N134 (Figure 1D). The D13 pocket had a C-score of 0.29 and TM-score of 0.98 and included F163, P478, F481, and F482 (Figure 1E). DNA polymerase produced a lower C-score (0.14) but a TM-score of 0.98; its broader pocket involved F109, H308, K309, K341, Y497, R498, A499, S500, T501, K504, K526, Y529, E530, G531, G532, V534, I663, N666, S667, Y669, G670, L671, G673, F674, N676, D752, T753, S803, K804-K806, Y807, K827, G828, T832, R833, R834, D835, S894, R895, H898, Y901, K902, N908, R928, K944, N947, I948, K949, V971, R975, and R1001 (Figure 1F).

3.3 Molecular docking and binding affinity

Among the 19 compounds screened against A42R, Scutellarein-7-O-diglucuronide ranked first at 8.265 kcal/mol, followed by Scutellarin (7.297), Baicalin (7.208), Norwogonoside (6.987), and Oroxyloside (6.987 kcal/mol). All exceeded the native PE8 value of 3.079 kcal/mol (Table 1; Figures 2A-2C).

For D13, Scutellarein-7-O-diglucuronide again ranked first (11.416 kcal/mol), followed by Baicalin (10.028), Norwogonoside (9.837), Oroxyloside (9.837), and Scutellarin (9.212 kcal/mol); rifampicin yielded 8.885 kcal/mol (Table 2). For DNA polymerase, Norwogonoside and Oroxyloside shared the highest value (10.022 kcal/mol), followed by Scutellarin (9.805), Baicalin (9.385), and Wogonoside (9.162 kcal/mol), compared with 8.681 kcal/mol for TTP (Table 3). Glycosylated flavonoids therefore dominated the leading ranks across all targets.

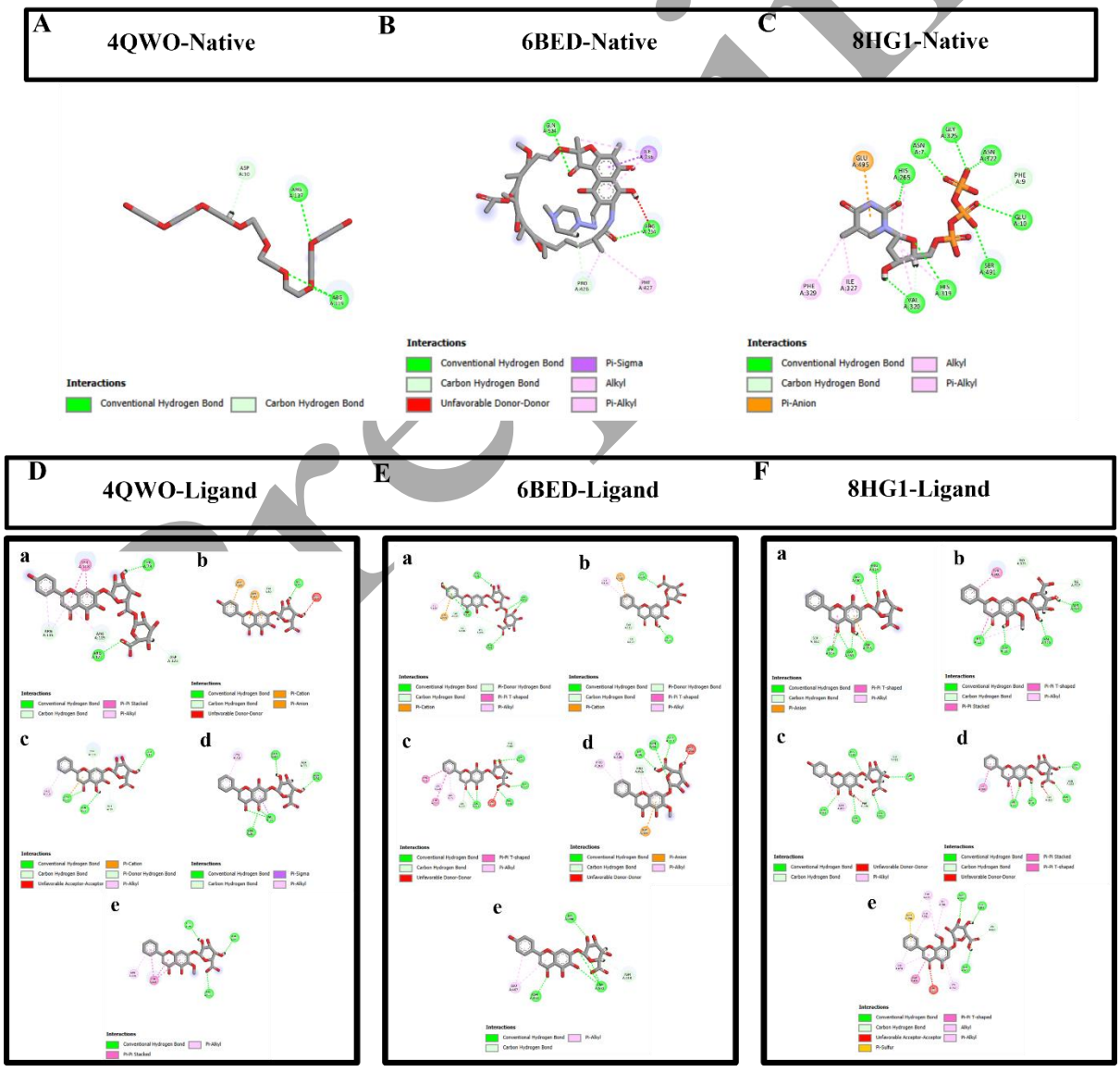

Figure 2. Post-docking analysis. Native-ligand complexes: (A) A42R-PE8, (B) D13-rifampicin, and (C) MPXV DNA polymerase-TTP. Protein–ligand interaction complexes of selected compounds from *Scutellaria baicalensis* with (D) A42R Profilin-like Protein, (E) scaffold protein D13, and (F) mpox virus DNA polymerase. Da) A42R Profilin-like-Scutellarein-7-O-diglucuronide. Db) A42R Profilin-like-Scutellarin. Dc) A42R Profilin-like-Baicalin. Dd) A42R Profilin-like-Norwogonoside. De) A42R Profilin-like-Oroxyloside. Ea) scaffold protein D13-Scutellarein-7-O-diglucuronide. Eb) scaffold protein D13-Baicalin. Ec) scaffold protein D13-Norwogonoside. Ed) scaffold protein D13-Oroxyloside. Ee) scaffold protein D13-Scutellarin. Fa) mpox virus DNA polymerase-Norwogonoside. Fb) mpox virus DNA polymerase-Oroxyloside. Fc) mpox virus DNA polymerase-Scutellarin. Fd) mpox virus DNA polymerase-Baicalin. Fe) mpox virus DNA polymerase-Wogonoside

Table 1. Binding energies of *S. baicalensis* compounds targeting the A42R profilin-like protein.

Ranking	**cid**	**compound**	**Binding energy (kcal/mol)**	**Dissoc. constant [pM]**
1.	177827718	Scutellarein-7-O-diglucuronide	8.265	874328.6
2.	185617	Scutellarin	7.297	4479485
3.	64982	Baicalin	7.208	5205542
4.	11597485	Norwogonoside	6.987	7558944
5.	14655552	Oroxyloside	6.987	7558944
6.	5320313	Baicalein-7-O-glucoside	6.976	7700594
7.	3084961	Wogonoside	6.794	10469645
8.	5281605	Baicalein	6.768	10939317
9.	5281697	Scutellarein	6.594	14673507
10.	3084390	5,6,4′-Trihydroxy-7-methoxyflavone	6.357	21890578
11.	5281665	Isoscutellarein	6.254	26046970

12.	5320315	Oroxylin A	6.19	29018158
13.	10355753	6,7,4′-Trihydroxyflavone	6.137	31733600
14.	5281674	Norwogonin	6.116	32878542
15.	466269	7,4′-Dimethoxyflavone	6.068	35653076
16.	5281607	Chrysin	6.068	35653076
17.	5320438	5,7-Dihydroxy-6,4′-dimethoxyflavone	6.041	37315416
18.	5281703	Wogonin	6.016	38923648
19.	5281894	7-Hydroxyflavone	5.932	44852468
20.	-	PE8 (Native Ligand)	3.079	5534304768

210

211 Table 2. Binding energies of *S. baicalensis* compounds targeting scaffold protein D13.

Ranking	**cid**	**compound**	**Binding energy (kcal/mol)**	**Dissoc. constant [pM]**
1.	177827718	Scutellarein-7-O-diglucuronide	11.416	4285.101
2.	64982	Baicalin	10.028	44604.48
3.	11597485	Norwogonoside	9.837	61572.02
4.	14655552	Oroxyloside	9.837	61572.02
5.	185617	Scutellarin	9.212	176813.1
6.	5281674	Norwogonin	9.025	242430.5
7.	-	Rifampicin (Native Ligand)	8.885	307049.6875
8.	3084961	Wogonoside	8.846	327941.2

9.	3084390	5,6,4′-Trihydroxy-7-methoxyflavone	8.834	334651
10.	5320313	Baicalein-7-O-glucoside	8.758	380452.9
11.	10355753	6,7,4′-Trihydroxyflavone	8.649	457297.6
12.	5281703	Wogonin	8.514	574321.8
13.	5320315	Oroxylin A	8.322	794132.8
14.	5281894	7-Hydroxyflavone	8.106	1143466
15.	5281697	Scutellarein	8.068	1219207
16.	5320438	5,7-Dihydroxy-6,4′-dimethoxyflavone	8.024	1313197
17.	5281665	Isoscutellarein	7.936	1523473
18.	5281605	Baicalein	7.922	1559901
19.	466269	7,4′-Dimethoxyflavone	7.644	2493870
20.	5281607	Chrysin	7.644	2493870

Table 3. Binding energies of *S. baicalensis* compounds targeting MPXV DNA polymerase.

Ranking	**cid**	**compound**	**Binding energy (kcal/mol)**	**Dissoc. constant [pM]**
1.	11597485	Norwogonoside	10.022	45058.48
2.	14655552	Oroxyloside	10.022	45058.48
3.	185617	Scutellarin	9.805	64988.98
4.	64982	Baicalin	9.385	132039.5
5.	3084961	Wogonoside	9.162	192382.2

6.	177827718	Scutellarein-7-O-diglucuronide	9.153	195326.9
7.	5320313	Baicalein-7-O-glucoside	8.833	335216.3
8.	5281697	Scutellarein	8.765	375984.4
9.	-	TTP (Native Ligand)	8.681	433254.0625
10.	5281894	7-Hydroxyflavone	8.629	472997.8
11.	5281665	Isoscutellarein	8.513	575291.9
12.	10355753	6,7,4′-Trihydroxyflavone	8.419	674203.8
13.	5281703	Wogonin	8.215	951316.8
14.	5281674	Norwogonin	8.189	993993.2
15.	3084390	5,6,4′-Trihydroxy-7-methoxyflavone	8.118	1120539
16.	5320315	Oroxylin A	8.071	1213050
17.	466269	7,4′-Dimethoxyflavone	7.99	1390761
18.	5281607	Chrysin	7.99	1390761
19.	5320438	5,7-Dihydroxy-6,4′-dimethoxyflavone	7.706	2246090
20.	5281605	Baicalein	7.558	2883451

3.4 Protein-ligand interactions

The PE8-A42R complex was dominated by hydrogen bonds with D10, R119, and R127, spatially consistent with the predicted D11 and R128 pocket region. The five leading A42R ligands formed broader combinations of hydrogen bonding, π-π stacking, π-alkyl, π-cation, π-anion, and π-sigma contacts (Figure 2Da-2Fe).

Unfavorable acceptor-acceptor or donor-donor contacts occurred in the A42R-Scutellarin and A42R-Baicalin complexes. By contrast, Scutellarein-7-O-diglucuronide lacked these contacts. A similar pattern occurred for D13: the two highest-ranked

ligands, Scutellarein-7-O-diglucuronide and Baicalin, had no identified unfavorable contacts, whereas rifampicin interacted unfavorably with R234.

For DNA polymerase, TTP and Norwogonoside formed mixed hydrogen-bonding and hydrophobic contacts. Oroxyloside reached the same docking energy through a distinct distribution of hydrogen bonds and hydrophobic interactions. Across the three targets, aromatic flavonoid rings supported frequent π-mediated contacts, while hydroxyl and glycoside groups contributed hydrogen-bonding capacity.

3.5 Molecular electrostatic potential

MEP surfaces showed heterogeneous charge distributions in all selected ligands (Figure 3A-3F). Electron-rich regions were concentrated around oxygen-containing hydroxyl and glycoside groups, whereas electron-deficient regions occurred near potential hydrogen donors. Norwogonoside displayed a broadly distributed negative potential, while Scutellarein-7-O-diglucuronide showed clearer spatial separation between electropositive and electronegative regions.

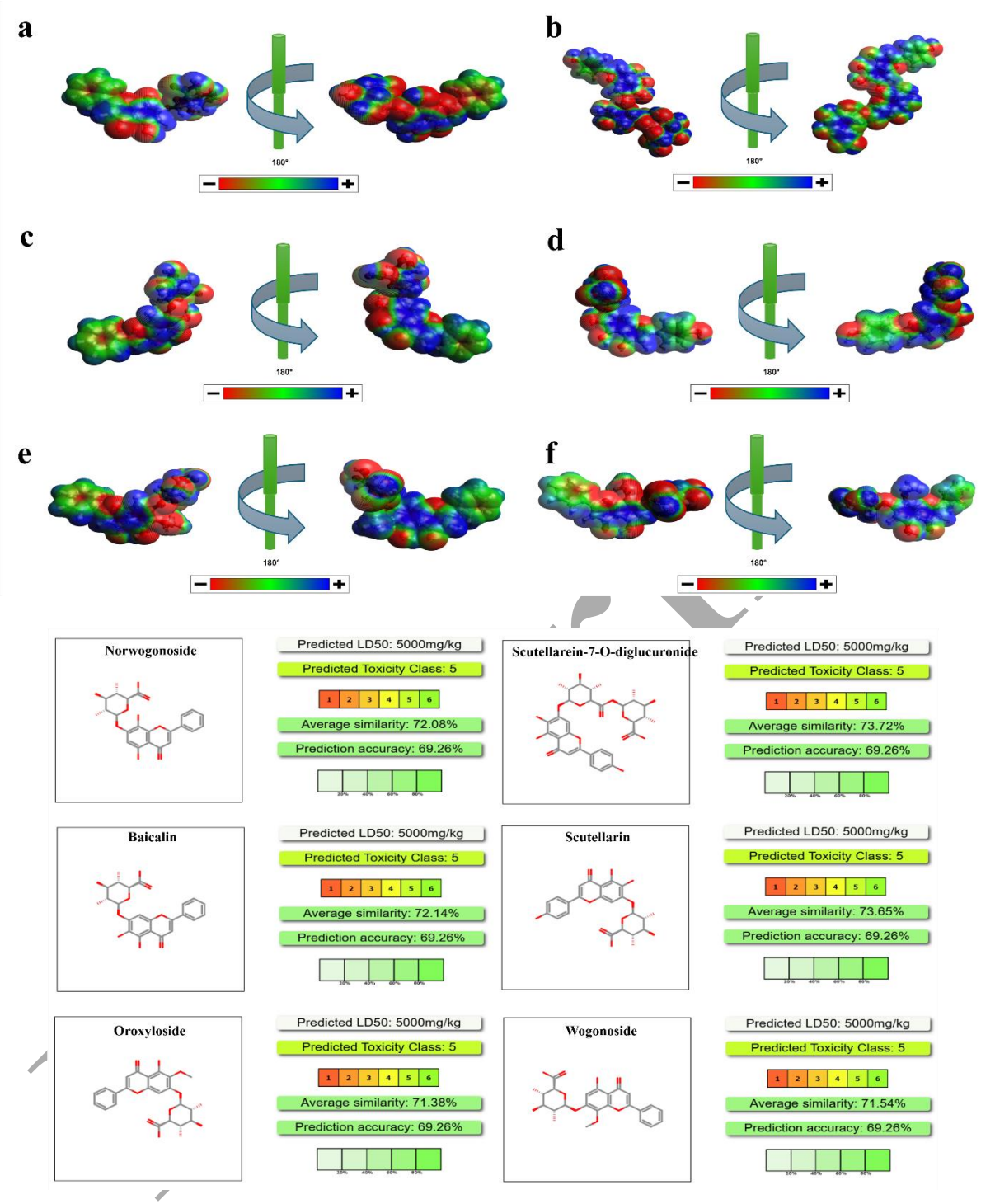

Figure 3. Analysis of selected candidate. MEP surfaces of (A) Scutellarein-7-O-diglucuronide, (B) Scutellarin, (C) Baicalin, (D) Norwogonoside, (E) Oroxyloside, and (F) Wogonoside. Red and blue denote negative and positive electrostatic potential, respectively. ProTox-3 toxicity assessment of selected *S. baicalensis* compounds.

Baicalin, Scutellarin, Oroxyloside, and Wogonoside showed comparable polar regions combined with aromatic surfaces. These distributions were consistent with the hydrogen-bonding and π-mediated interactions identified in docking poses.

246

247 3.6 Toxicity prediction

248 All six selected compounds had a predicted LD50 of 5,000 mg/kg and were assigned
249 to toxicity class 5 (Figure 3). Norwogonoside, Scutellarein-7-O-diglucuronide,
250 Baicalin, and Scutellarin were inactive for hepatotoxicity, neurotoxicity,
251 cardiotoxicity, immunotoxicity, mutagenicity, and cytotoxicity (Table 4).

252 Oroxyloside was predicted active for cardiotoxicity and immunotoxicity, and
253 Wogonoside was predicted active for cardiotoxicity; all remaining endpoints were
254 inactive. Accordingly, Scutellarein-7-O-diglucuronide combined the highest A42R
255 and D13 docking energies with the most favorable predicted toxicity pattern, while
256 Norwogonoside showed the corresponding combination for DNA polymerase.

257

258 Table 4. ProTox-3 toxicity predictions for selected *S. baicalensis* compounds.

Compound	CID	Hepatotoxicity	Neurotoxicity	Cardiotoxicity	Immunotoxicity	Mutagenicity	Cytotoxicity
Norwogonoside	11597485	Inactive	Inactive	Inactive	Inactive	Inactive	Inactive
Scutellarein-7-O-diglucuronide	177827718	Inactive	Inactive	Inactive	Inactive	Inactive	Inactive
Baicalin	64982	Inactive	Inactive	Inactive	Inactive	Inactive	Inactive
Scutellarin	185617	Inactive	Inactive	Inactive	Inactive	Inactive	Inactive
Oroxyloside	14655552	Inactive	Inactive	Active	Active	Inactive	Inactive
Wogonoside	3084961	Inactive	Inactive	Active	Inactive	Inactive	Inactive

259

260 3.7 Molecular dynamics

261 RMSD histograms from the 10 ns trajectories revealed target- and ligand-dependent
262 conformational distributions (Figure 4Aa-4Ce). A42R-Scutellarein-7-O-diglucuronide

showed dominant populations near 5-10 and 15-18 Å, whereas A42R-Scutellarin was concentrated near 4-5 Å. Other A42R complexes were multimodal. D13-Scutellarein-7-O-diglucuronide was centered at 7-9 Å with a higher-RMSD tail; D13-Baicalin and D13-Scutellarin were comparatively narrow, while D13-Norwogonoside and D13-Oroxyloside were broader. DNA polymerase-Norwogonoside was centered near 7-9 Å, whereas Oroxyloside and Baicalin extended toward 15-18 Å.

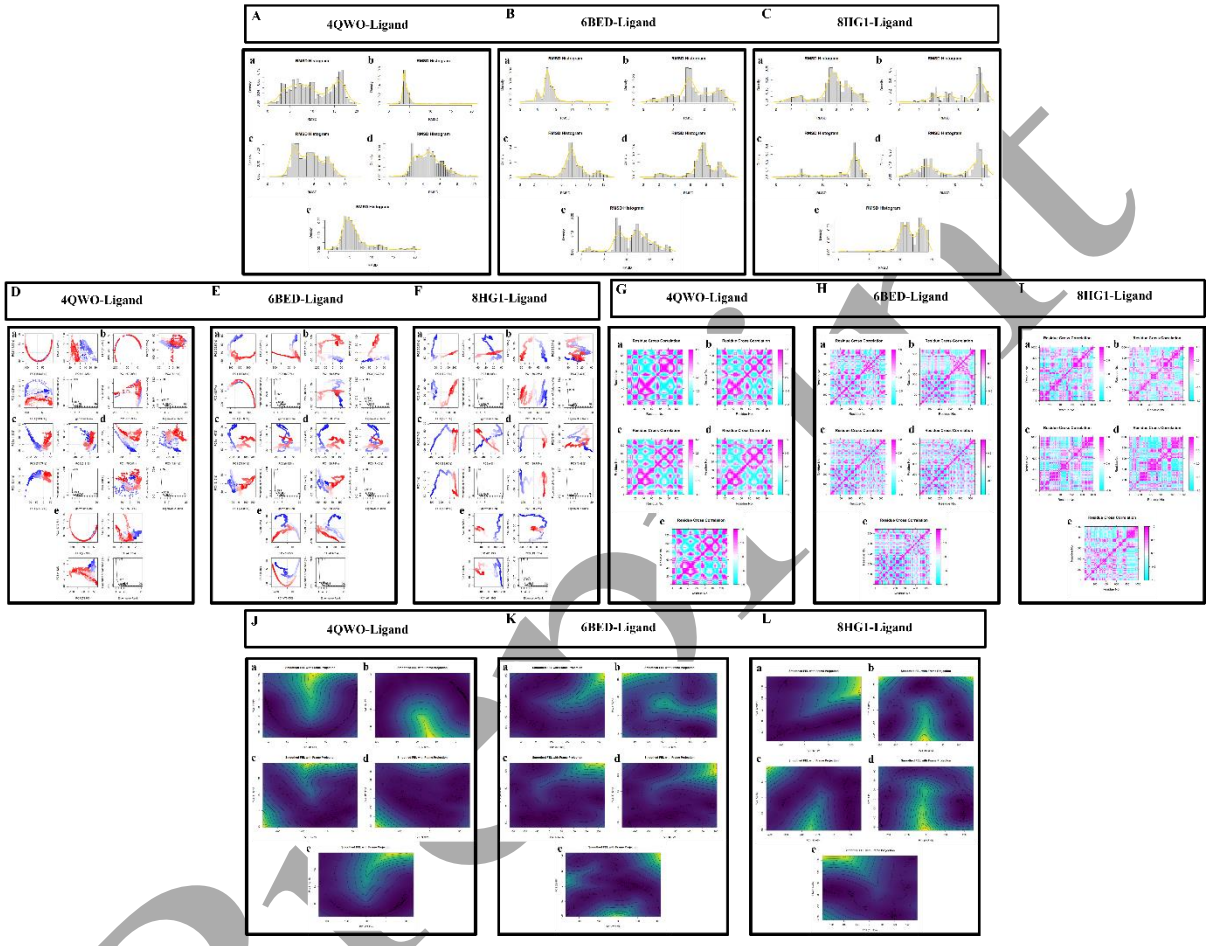

Figure 4. Post-MD analyses of selected MPXV protein–ligand complexes. RMSD distributions (A–C), principal component analysis (PCA; D–F), dynamic cross-correlation matrices (DCCM; G–I), and free-energy landscapes (FEL; J–L) are shown for A42R (A, D, G, J), D13 (B, E, H, K), and MPXV DNA polymerase (C, F, I, L). Within each A42R panel, subpanels a–e represent Scutellarein-7-O-diglucuronide, Scutellarin, Baicalin, Norwogonoside, and Oroxyloside, respectively. Within each D13 panel, subpanels a–e represent Scutellarein-7-O-diglucuronide, Baicalin, Norwogonoside, Oroxyloside, and Scutellarin, respectively. Within each DNA polymerase panel, subpanels a–e represent Norwogonoside, Oroxyloside, Scutellarin, Baicalin, and Wogonoside, respectively.

PCA showed that A42R complexes were largely governed by PC1 (67.99-81.63%; Figure 4Da-4Fe). A42R-Scutellarein-7-O-diglucuronide had the largest PC1

contribution (81.63%), followed by PC2 (14.05%) and PC3 (1.22%). For D13, Scutellarein-7-O-diglucuronide and Baicalin had similar PC1 contributions (58.66% and 58.68%), while D13-Scutellarin reached 76.05%. DNA polymerase-Baicalin and DNA polymerase-Scutellarin had strongly dominant PC1 values of 89.73% and 83.95%, respectively; DNA polymerase-Oroxyloside showed a broader distribution (PC1 56.26%; PC2 35.31%).

DCCM maps were dominated by positively correlated residue motions, with localized anti-correlated regions (Figure 4Ga-4Ie). DNA polymerase complexes displayed denser correlation networks than the smaller targets. FEL projections generally contained one principal low-energy basin, although several A42R and D13 systems showed secondary minima consistent with their multimodal RMSD distributions (Figure 4Ja-4Le).

3.8 NMA, RIN, and Protein Contact Atlas results

NMA of the leading complex for each target showed preserved elastic connectivity with localized flexible regions (Figure 5A-5C). Eigenvalues were 1.259931×10^{-3} for A42R-Scutellarein-7-O-diglucuronide, 8.556070×10^{-6} for D13-Scutellarein-7-O-diglucuronide, and 3.408562×10^{-5} for DNA polymerase-Norwogonoside. The lower values for D13 and DNA polymerase indicated lower deformation-energy requirements. Protein Contact Atlas chord plots and centrality matrices summarized the corresponding secondary-structure and residue-network connectivity (Figure 5D-5F).

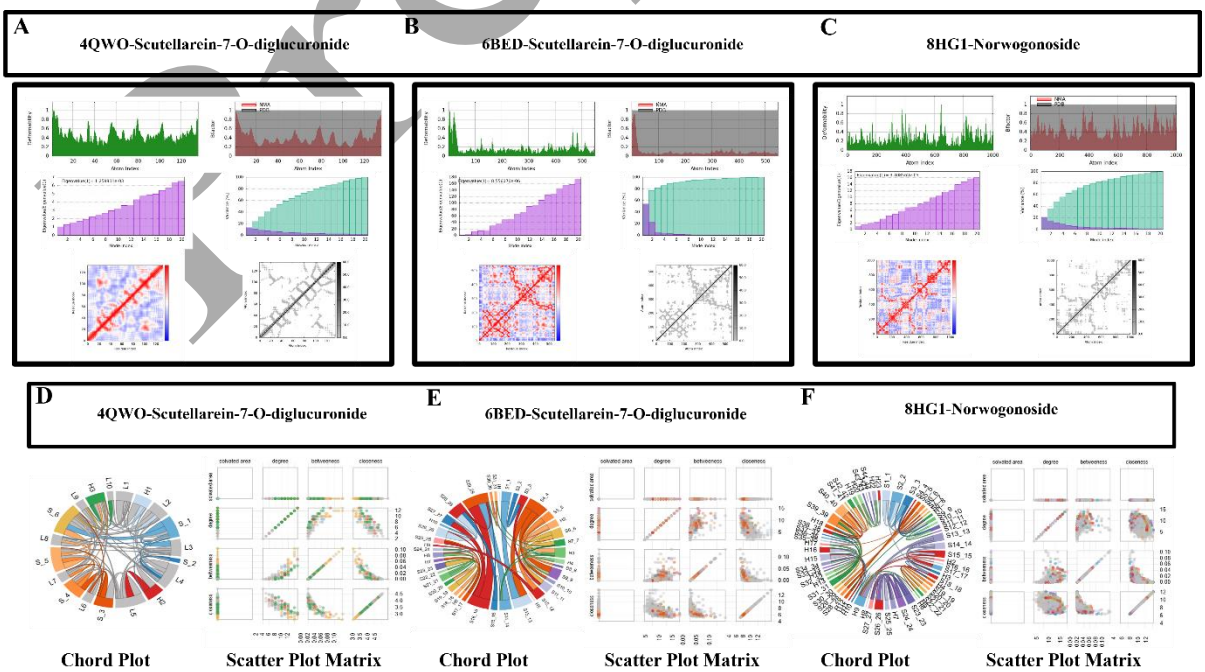

Figure 5. iMODS NMA profiles for the leading A42R, D13, and MPXV DNA polymerase complexes after 10 ns simulation, including deformability, B-factor, eigenvalue, variance, covariance, and elastic-network outputs. PCAt analysis showing chord plot connectivity among secondary structural elements and scatter plot matrix of residue network statistics, including degree centrality, betweenness, closeness, and solvent accessible area for the top protein–ligand complexes.

RIN analysis showed that main-chain hydrogen bonds represented 86.81%, 76.27%, and 84.99% of categorized interactions in the A42R, D13, and DNA polymerase leading complexes, respectively. Mean hydrogen-bond distances were 2.9902, 2.9868, and 2.9989 Å, and mean π-cation distances were 4.6639, 4.2968, and 3.992 Å. DNA polymerase-Norwogonoside had the lowest reported mean hydrogen-bond energy (-0.1204 kJ/mol), compared with -0.0858 and -0.0002 kJ/mol for A42R and D13 (Figure 6A-6O).

A

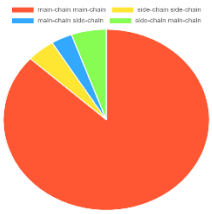

main-chain main-chain	side-chain side-chain	main-chain side-chain	side-chain main-chain
86.81	4.40	3.30	5.49

B

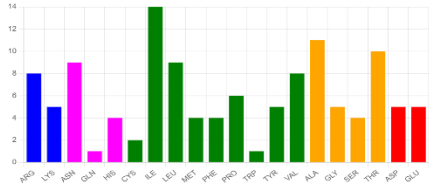

C

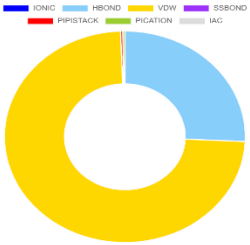

IONIC	HBOND	VDW	SSBOND	PIPISTACK	PICATION	IAC
0	91	261	0	1	1	0

D

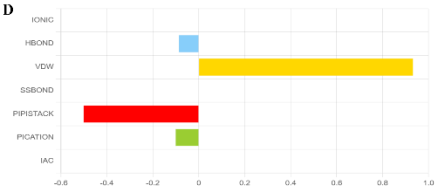

E

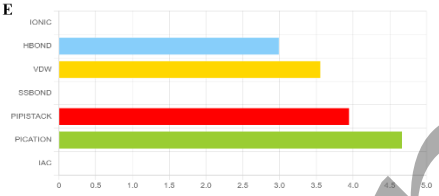

F

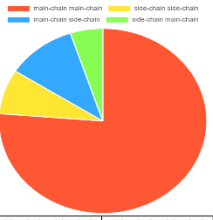

main-chain main-chain	side-chain side-chain	main-chain side-chain	side-chain main-chain
76.27	7.80	10.85	5.08

G

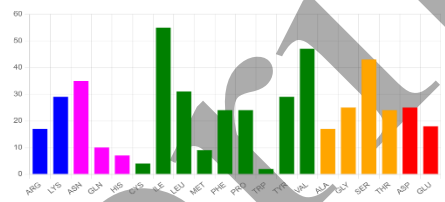

H

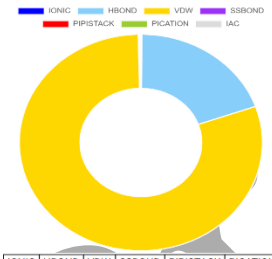

IONIC	HBOND	VDW	SSBOND	PIPISTACK	PICATION	IAC
2	295	1214	0	2	3	0

I

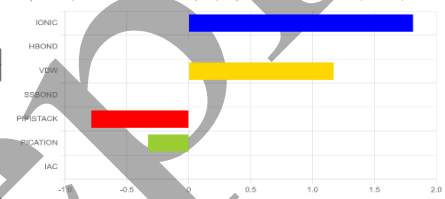

J

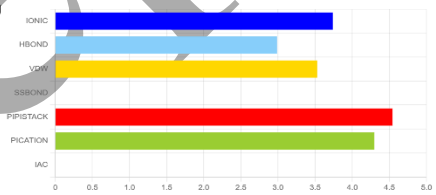

K

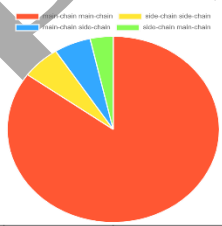

main-chain main-chain	side-chain side-chain	main-chain side-chain	side-chain main-chain
84.99	5.87	5.61	3.52

L

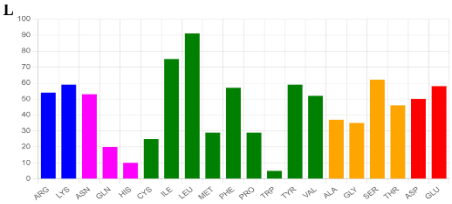

M

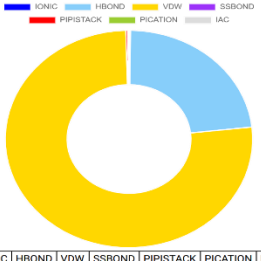

IONIC	HBOND	VDW	SSBOND	PIPISTACK	PICATION	IAC
7	766	2541	0	8	5	0

N

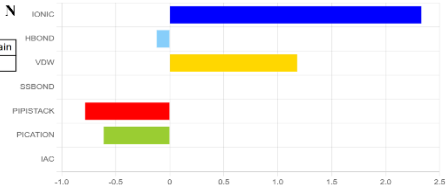

O

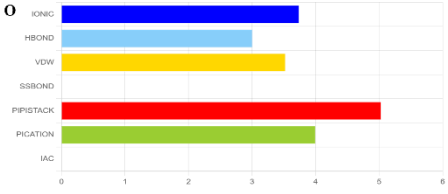

Figure 6. Residue interaction network analysis of the leading MPXV protein–ligand complexes. A42R–Scutellarein-7-O-diglucuronide is shown in panels A–E, D13–Scutellarein-7-O-diglucuronide in F–J, and MPXV DNA polymerase–Norwogonoside in K–O. For each complex, the panels present hydrogen-bond distribution, residue count, bond count, mean interaction energy (kJ/mol), and mean interaction distance, respectively..

4. Discussion

Our study performed receptor validation, which supported the geometric suitability of the initial structures, with more than 90% of residues located in favored Ramachandran regions [15]. However, the confidence level of the predicted binding sites differed among the targets. The higher C-score for A42R provided stronger support for the predicted binding pocket compared with D13 and DNA polymerase, although the latter two proteins showed high TM-score values [16].

This study showed that the ranking of the tested compounds was dependent on the MPXV target. We observed that Scutellarein-7-O-diglucuronide was more favorable for A42R and D13, which are associated with host-related viral functions and virion morphogenesis, respectively, whereas Norwogonoside was more favorable for DNA polymerase, an essential component of genome replication. This pattern supports the scientific rationale for applying multi-target screening across different stages of the MPXV life cycle and may reduce dependence on a single viral mechanism [17]. Nevertheless, these predictions do not yet demonstrate simultaneous inhibition, synergistic effects, or antiviral efficacy.

In general, we observed that glycosylated flavonoids showed better performance than the reference ligands. Chemically, this may be explained by the presence of hydroxyl groups and glycosidic oxygen atoms, which support extensive hydrogen bond formation, while the aromatic scaffold allows π-mediated interactions. However, docking scores remain model-dependent, and differences in target structures, software, scoring functions, protonation states, solvation treatment, and conformational sampling limit direct comparisons across studies [18,19]. Our findings are generally consistent with previous reports describing favorable polyphenol binding to MPXV proteins, including punicalagin against E8 [20]. Scutellarein-7-O-diglucuronide and Norwogonoside also showed favorable predicted toxicity profiles; however, their high polarity may limit compound permeability and exposure. Therefore, cellular toxicity, metabolic stability, pharmacokinetic characteristics, and formulation requirements should be evaluated before these compounds can be considered viable antiviral candidates [18–21].

We observed that the selected complexes with favorable docking profiles did not necessarily adopt rigid conformations during the molecular dynamics simulations. Instead, the multimodal RMSD distributions, the presence of secondary minima in the free-energy landscapes, and the dominant contributions of PC1 indicated

conformational adaptation within organized patterns of collective motion. We therefore emphasize that these findings remain predictive in nature, and that the 10 ns coarse-grained simulations were designed for comparative screening rather than for establishing long-term stability, equilibrium binding behavior, or binding free energy. We also acknowledge additional uncertainty arising from the restricted chemical library of 19 reported *S. baicalensis* constituents, the lower binding-site confidence associated with D13 and DNA polymerase, and the model-dependent nature of the docking and toxicity predictions. Accordingly, the proposed multi-target activity requires further validation through longer and independently replicated atomistic simulations, biophysical binding measurements, target-specific inhibition assays, and cell-based antiviral studies. Overall, this study should be regarded as a hypothesis-generating computational framework for prioritizing Scutellarein-7-O-diglucuronide and Norwogonoside for subsequent experimental evaluation.

5. Conclusion

This study identified Scutellarein-7-O-diglucuronide as the leading candidate for A42R and D13, whereas Norwogonoside was prioritized for MPXV DNA polymerase based on their combined docking, interaction, toxicity, and conformational profiles. The target-dependent performance of these compounds supports the potential value of a multi-target strategy directed toward viral processes associated with host interaction, virion morphogenesis, and genome replication. From a practical perspective, these findings provide a focused basis for selecting natural-product-derived candidates for subsequent biochemical and cell-based evaluation, thereby reducing the number of compounds requiring resource-intensive experimental screening. Their translational potential, however, will depend on confirmation of direct target binding, functional inhibition, antiviral efficacy, cellular safety, membrane permeability, metabolic stability, and intracellular exposure. Future studies should therefore integrate longer atomistic simulations with biophysical assays, target-specific inhibition studies, pharmacokinetic evaluation, and MPXV or appropriate orthopoxvirus infection models. Overall, the present workflow offers a hypothesis-generating framework for advancing Scutellarein-7-O-diglucuronide and Norwogonoside from computational prioritization toward experimental antiviral validation.

6. Acknowledgements.

Not Applicable.

7. Authors' Contribution

WN: Conceptualization, Data curation, Formal analysis, Investigation, Methodology, Software, Visualization, Writing – original draft, Writing – review & editing.

GMG: Conceptualization, Investigation, Methodology, Software, Visualization, Writing – original draft, Writing – review & editing.

RAPI: Data curation, Methodology, Formal analysis, Validation, Writing – review & editing.

FS: Data curation, Formal analysis, Validation, Writing – review & editing.

EF: Data curation, Formal analysis, Validation, Writing – review & editing.

JES: Data curation, Formal analysis, Validation, Writing – review & editing.

SW: Data curation, Formal analysis, Validation, Writing – review & editing.

WW: Data curation, Formal analysis, Validation, Writing – review & editing.

8. Conflict of Interest

The authors declare that they have no known competing financial interests or personal relationships that could have appeared to influence the work reported in this paper.

9. Ethical approval

Not applicable. This research did not involve human participants or animal experiments.

10. Funding

Not applicable.

11. Data Availability

Data supporting the findings of this study are available upon reasonable request from the corresponding author.

12. References

[1] Karagoz A, Tombuloglu H, Alsaeed M, Tombuloglu G, AlRubaish AA, Mahmoud A, et al. Monkeypox (mpox) virus: Classification, origin, transmission, genome organization, antiviral drugs, and molecular diagnosis. J Infect Public Health 2023;16:531–41. https://doi.org/10.1016/j.jiph.2023.02.003.

[2] Dobhal K, Ghildiyal P, Ansori ANM, Jakhmola V. An International Outburst of New Form of Monkeypox Virus. J Pure Appl Microbiol 2022;16:3013–24. https://doi.org/10.22207/JPAM.16.SPL1.01.

[3] Ogoina D, Dalhat MM, Denue BA, Okowa M, Chika-Igwenyi NM, Yusuff HA, et al. Clinical characteristics and predictors of human mpox outcome during the

2022 outbreak in Nigeria: a cohort study. Lancet Infect Dis 2023;23:1418–28. https://doi.org/10.1016/S1473-3099(23)00427-9.

[4] Prajapati A, Jella R, Dendi MR, Salla S, Mukherjee S, Bayry J, et al. Understanding Monkeypox Virus Evolution, Host-Pathogen Interactions, and Therapeutic Advances. Rev Med Virol 2026;36. https://doi.org/10.1002/rmv.70103.

[5] La Frazia S, Garbuglia AR, Pauciullo S, Zulian V, Del Porto P. Genomic variability and immunological aspects involved in response to MPXV infection. Front Pharmacol 2025;16. https://doi.org/10.3389/fphar.2025.1665830.

[6] Ashley CN, Broni E, Wood CM, Okuneye T, Ojukwu M-PT, Dong Q, et al. Identifying potential monkeypox virus inhibitors: an in silico study targeting the A42R protein. Front Cell Infect Microbiol 2024;14. https://doi.org/10.3389/fcimb.2024.1351737.

[7] Patil H, Kute P, Bonde C, Bhole R, Chaudhari S, Gawad J, et al. Repurposing of FDA-approved antiviral drugs against monkey pox virus: A computational targeting of VP39 methyl transferase. In Silico Research in Biomedicine 2026;2:100259. https://doi.org/10.1016/j.insi.2026.100259.

[8] Tarbouriech N, Ducournau C, Hutin S, Mas PJ, Man P, Forest E, et al. The vaccinia virus DNA polymerase structure provides insights into the mode of processivity factor binding. Nat Commun 2017;8:1455. https://doi.org/10.1038/s41467-017-01542-z.

[9] HUANG Q, WANG M, WANG M, LU Y, WANG X, CHEN X, et al. Scutellaria baicalensis: a promising natural source of antiviral compounds for the treatment of viral diseases. Chin J Nat Med 2023;21:563–75. https://doi.org/10.1016/S1875-5364(23)60401-7.

[10] Ajmal A, Mahmood A, Hayat C, Hakami MA, Alotaibi BS, Umair M, et al. Computer-assisted drug repurposing for thymidylate kinase drug target in monkeypox virus. Front Cell Infect Microbiol 2023;13. https://doi.org/10.3389/fcimb.2023.1159389.

[11] Minasov G, Inniss NL, Shuvalova L, Anderson WF, Satchell KJF. Structure of the Monkeypox virus profilin-like protein A42R reveals potential functional differences from cellular profilins. Acta Crystallogr F Struct Biol Commun 2022;78:371–7. https://doi.org/10.1107/S2053230X22009128.

[12] Garriga D, Headey S, Accurso C, Gunzburg M, Scanlon M, Coulibaly F. Structural basis for the inhibition of poxvirus assembly by the antibiotic rifampicin. Proceedings of the National Academy of Sciences 2018;115:8424–9. https://doi.org/10.1073/pnas.1810398115.

[13] Peng Q, Xie Y, Kuai L, Wang H, Qi J, Gao GF, et al. Structure of monkeypox virus DNA polymerase holoenzyme. Science (1979) 2023;379:100–5. https://doi.org/10.1126/science.ade6360.

[14] Chanchal DK, Singh K, Bhushan B, Chaudhary JS, Kumar S, Varma AK, et al. An updated review of Chinese skullcap (Scutellaria baicalensis): Emphasis on phytochemical constituents and pharmacological attributes. Pharmacological Research - Modern Chinese Medicine 2023;9:100326. https://doi.org/10.1016/j.prmcm.2023.100326.

[15] Pitchiah S, Ganapathy D, Kamala K. Virulence and antimicrobial resistance gene profiling in multidrug-resistant Pseudomonas aeruginosa with evaluation of levofloxacin and amikacin therapy. Microb Pathog 2026;213:108334. https://doi.org/10.1016/j.micpath.2026.108334.

[16] Zhao J, Cao Y, Zhang L. Exploring the computational methods for protein-ligand binding site prediction. Comput Struct Biotechnol J 2020;18:417–26. https://doi.org/10.1016/j.csbj.2020.02.008.

[17] Arasu MV, Vijayaragavan P, Purushothaman S, Rathi MA, Al-Dhabi NA, Gopalakrishnan VK, et al. Molecular docking of monkeypox (mpox) virus proteinase with FDA approved lead molecules. J Infect Public Health 2023;16:784–91. https://doi.org/10.1016/j.jiph.2023.03.004.

[18] Berisha A. Structure–Activity Analysis and DNA Binding Potential of Nitro-PAHs: A Combined Virtual Screening, QSAR, and Toxicity Profiling Approach. Biointerface Res Appl Chem 2025;15. https://doi.org/10.33263/BRIAC156.079.

[19] Astakala RV, Preet G, Haj Hasan A, Desai R, Alfurayh M, Ebel R, et al. Computational repurposing of polyphenols for anti-Mpoxviral activity. In Silico Pharmacol 2025;13:65. https://doi.org/10.1007/s40203-025-00345-1.

[20] Lailiyyah H, Lisdiana L. Uji Aktivitas Antibakteri Senyawa Aktif Temu Kunci (Boesenbergia rotunda) Terhadap Mycobacterium tuberculosis Secara In Silivo. LenteraBio : Berkala Ilmiah Biologi 2023;12:132–49. https://doi.org/10.26740/lenterabio.v12n2.p132-149.

[21] Aziz RAZ, Purnama ER. In silico Analysis of the Potential of Red Betel (Piper crocatum) Active Compounds as Anti-Inflammatory Drug Candidate. LenteraBio: Berkala Ilmiah Biologi 2024;13.

499

500

501